ACS APPLIED MATERIALS & INTERFACES

Research Article

www.acsami.org

Efficient Quantum Dot Light-Emitting Diodes by Controlling the Carrier Accumulation and Exciton Formation

Wenyu Ji,[†] Ye Tian,[§] Qinghui Zeng,[†] Songnan Qu,[†] Ligong Zhang,[†] Pengtao Jing,*[,†] Jia Wang,[†] and Jialong Zhao*[,‡]

[†]State Key Laboratory of Luminescence and Applications, Changchun Institute of Optics, Fine Mechanics and Physics, Chinese Academy of Sciences, Changchun 130033, China

[‡]Key Laboratory of Functional Materials Physics and Chemistry of the Ministry of Education, Jilin Normal University, Siping 136000, China

[§]Department of Applied Biology and Chemical Technology, the Hong Kong Polytechnic University, Hung Hom, Kowloon, Hong Kong

ABSTRACT: The performances and spectroscopic properties of CdSe/ZnS quantum dot light-emitting diodes (QD-LEDs) with inserting a thickness-varied 1,3,5-tris(*N*-phenylbenzimidazole-2-yl)benzene (TPBi) layer between the QD emission layer and 4,4-*N,N*-dicarbazole-biphenyl (CBP) hole transport layer (HTL) are studied. The significant enhancement in device peak efficiency is demonstrated for the device with a 3.5 nm TPBi interlayer. The photoluminescence lifetimes of excitons formed within QDs in different devices are also measured to understand the influence of electric field on the QD emission dynamics process and device efficiency. All the excitons on QDs at different devices have nearly the same lifetime even though at different bias. The improvement of device performance is attributed to the separation of charge carrier accumulation interface from the exciton formation zone, which suppresses exciton quenching caused by accumulated carriers.

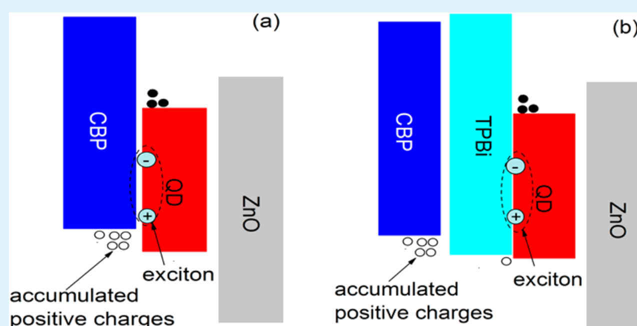

KEYWORDS: *quantum dot light-emitting diodes, carrier accumulation interface, exciton quenching, inverted structure, exciton formation zone*

INTRODUCTION

The quantum dot light-emitting diodes (QD-LEDs), because of their unique potential properties, including QD size-tunable emission-wavelength from visible to near-infrared, high efficiency, cost-effective fabrication techniques compatible with solution-processed methods, and high color purity, have attracted much attention and are considered as one of the most practical candidates for flat panel displays and solid-state lighting sources,[1−11] offering significant advantages over organic LEDs (OLEDs).[12,13] Since the first QD-LED was demonstrated,[4] there have been numerous effort and progress to improve the device performance by optimizing both the QD materials and the device architectures.[1−5,14−18] A number of approaches to fabricate efficient QD-LEDs have been reported, including device structures that include organic, inorganic and hybrid approaches to the formation of charge transport and injection layers. Especially, the recent demonstration of QD-LEDs with high performance close to (even exceeding) that of fluorescent organic LEDs (OLEDs)[1,2] further encourages the interest in developing QD-LEDs for practical applications. This important breakthrough has opened up opportunity to fabricate high efficient QD-LEDs to meet the commercial request. However, despite these recent progresses, there are still many issues in QD-LEDs for the practical applications: (1) low device efficiency in the practicable brightness region; (2) non-negligible parasitic electroluminescence (EL) emission from the adjacent conjugated organic layers or surface-trap states of QDs,[7] mainly due to inefficient carrier injection into the QDs or/and poor electron−hole balance; and (3) exciton quenching due to multicarrier or energy transfer processes. It is convinced that the exciton quenching processes can be dramatically decreased by subtly designing the QD materials and device structure.[3,19] Recently, the role of multicarrier effect, also referred to as Auger recombination, is studied by carefully adjusting the QD material structure in QD-LEDs.[3] It is concluded that the QD-LED efficiency is not solely dependent on single-exciton photoluminescence (PL) quantum yield, even at low current (or low exciton densities). The exciton quenching processes should deserve much intensive investigation to deeply understand the luminescence mechanism in QD-LEDs. However, to date, the physics underlying the QD-LEDs, and specifically the factors that limit their performance,

Received: May 28, 2014
Accepted: July 15, 2014
Published: July 15, 2014

ACS Publications © 2014 American Chemical Society

dx.doi.org/10.1021/am5033567 | *ACS Appl. Mater. Interfaces* 2014, 6, 14001−14007

is still unclear and need to be greatly investigated by optimizing the QD materials and device architectures. At present, the typical QD-LEDs are comprised of a QD emission layer sandwiched between hole-transport layer (HTL) and electron transport layer. As we know, two mechanisms have been proposed to explain the EL processes of QD-LEDs. The first one is that carriers transported through charge-transport layers are directly injected into QDs, where they can form excitons that then can radiatively recombine. For the second one, the excitons are formed on the adjacent organic molecules surrounding the QD film that then resonantly transfer the exciton energy to QDs. No matter which mechanism is working in the QD-LEDs, the exciton recombination zone is always at or near the QD/HTL interface. In other words, the carriers (electrons and holes) are accumulated at this interface and some of them will form the excitons within QDs or/and HTL. And the excess carriers form the accumulated space charges. The space charges, also named as charging radical (mainly are radical cations considering the carrier mobility of all the materials in QD-LEDs regardless of conventional or inverted device structures) will quench the excitons and decrease the device performance, which has been intensely investigated in OLEDs.[20] Similarly, the accumulated charges should exist at the QD/HTL interface in QD-LEDs. To date, there are not any reports on this phenomenon in QD-LEDs. Eliminating exciton quenching caused by the accumulated space charges remains a significant challenge in common device designs. However, it is still possible to reduce the radical cation accumulation by rational device design, such as controlling the energy-level alignment at the HTL/emission-layer interface to separate the charge accumulation interface from the exciton formation zone, which should prevent the associated exciton quenching processes and improve the device performance.

In this study, we fabricated a set of QD-LEDs with the structure of ITO/ZnO/QDs/interlayer/CBP/MoO_3/Al. The thickness of TPBi interlayer is varied from 0 to 7 nm. The interlayer plays a role in separating the charge accumulation interface from exciton formation zone, consequently decreasing the exciton quenching caused by accumulated charges. The performance of devices with TPBi interlayer is enhanced and an enhancement of 46% for device peak efficiency is achieved with a 3.5 nm TPBi interlayer. The influence of electric field distribution is assessed by the transient PL dynamics of QDs in different devices. All the results demonstrate that the improved performance of devices does not originate from the change of electric field but from the suppression of exciton quenching processes induced by accumulated charges. Clearly, the traditional concept of confining holes and electrons at the emission interface may not be an optimal device design option. Here, we for the first time report the exciton quenching due to the accumulated carriers in QD-LEDs and propose a strategy to decrease this quenching process to improve the device performance.

EXPERIMENTAL DETAILS

The QD-LEDs consist of glass coated ITO/ZnO (45 nm)/QDs (30 nm)/TPBi (*x* nm)/CBP (50 nm)/MoO_3 (5 nm)/Al (100 nm). The ZnO, QDs, CBP, and MoO_3 are used as electron transport layer (ETL), emission layer, HTL, and hole injection layer, respectively. The thickness of TPBi layer is varied from 0 to 7 nm for different devices, Device A (0 nm), Device B (0.5 nm), Device C (2 nm), Device D (3.5 nm), and Device E (7 nm). Device A is a conventional device without the TPBi interlayer. Before fabricating the devices, the ITO substrates were ultrasonically cleaned with a standard regiment of acetone, ethanol, deionized water, and isopropanol followed by an ex situ UV ozone treatment in air for 5 min. The ZnO nanoparticles were spin-coated onto the cleaned ITO substrates at 2000 rpm from a 25 mg/mL ZnO butanol solution and then annealed at 100 °C for 30 min in a glovebox (MBRAUN) to obtain a highly conductive layer with a thickness of about 45 nm. Until the ZnO coating substrates cooled to the room temperature, the QD layer was deposited on ZnO film by spin-coating QD toluene solution (5 mg/mL) at 2000 rpm and then annealed at 70 °C for 30 min in the same glovebox (MBRAUN). The substrates were then quickly loaded into the vacuum chamber and the rest of the device fabrication was finished without breaking the vacuum. All films were deposited at a pressure below 4×10^{-6} Torr. Detailed processes of fabrication and measurement for QD-LEDs have been described in our previous papers.[21,22] The red CdSe/ZnS core−shell QDs and ZnO nanoparticles were synthesized using a method from a previous report.[2,23] CBP, FIrpic, and TPBi were purchased from LumTec, and PEDOT:PSS was purchased from H. C. Starck. All the materials were used as received without any further purification. In the same vacuum chamber, the Al cathode lines with a width of 2.5 mm were deposited orthogonally to the ITO anode lines (the width is 2 mm) to form a 5 mm^2 active area.

The room-temperature absorption spectrum was measured with an ultraviolet/visible spectrometer (UV 1700, Shimadzu) and the PL spectrum of the QDs in toluene was collected by a Hitachi F-4500 spectrophotometer under an excitation wavelength of 400 nm. Time-resolved photoluminescence (TRPL) measurements were carried out with Edinburgh Instruments FL920 spectrometer, utilizing a 450 nm excitation light source. The transmission electron microscopy (TEM) images were recorded on a Philips TECNAI G2. The morphology of the ZnO and QDs films on ITO substrates was characterized by scanning electron microscope (SEM) (Hitachi S4800).

RESULTS AND DISCUSSION

It has been demonstrated that the QDs with a thick shell is beneficial to the device performance, such as efficiency and stability,[23−25] so here we also adopted CdSe/ZnS core−shell QDs with a ∼ 2.4 nm ZnS shell as the emission layer to fabricate QD-LEDs. Figure 1a shows the absorption and PL spectra of the CdSe/ZnS QDs (in toluene) used in our devices. The PL peak is located at 618 nm and the full-width at half-maximum (fwhm) is 37 nm. The quantum yield of CdSe/ZnS core−shell QDs is 65% in solid powder form measured with an integrating sphere. The high-resolution TEM image of the CdSe/ZnS QDs is shown in Figure 1b. High crystallinity of individual QDs is obtained and the average diameter of the QDs is ∼8 nm with a 3.0 nm CdSe core and 8 monolayer (∼2.4 nm) ZnS shell. The structure of the devices is schematically shown in Figure 2a, QD emission layer is sandwiched between a ZnO nanoparticle ETL and CBP HTL for the conventional device. The TPBi with different thicknesses is introduced at the QDs/CBP interface to assess its effect on device performance. The flat energy levels of the materials used in our study are shown in Figure 2b. Considering the energy level alignment, the exciton recombination zone should be at the QD/CBP interface for the conventional device. As we know, the hole mobility of CBP film is about 1.0×10^{-3} cm^2 V^{-1} s^{-1} and the electron mobility of ZnO nanoparticle film is $\sim 1.3 \times 10^{-3}$ cm^2 V^{-1} s^{-1}.[2,26] Moreover, it is commonly accepted that the electron mobility of QD layer is lower than that of general organic and inorganic semiconductor materials. As a result, the hole density at the QD/CBP interface will be higher than electron density because of the low electron mobility of QD layer, which will lead to the formation of space charges (radical cations) at the QD/CBP interface and hence quenching the excitons as reported in OLEDs.[20] TPBi is a typical n-type matrix material and the electron mobility of TPBi is of the

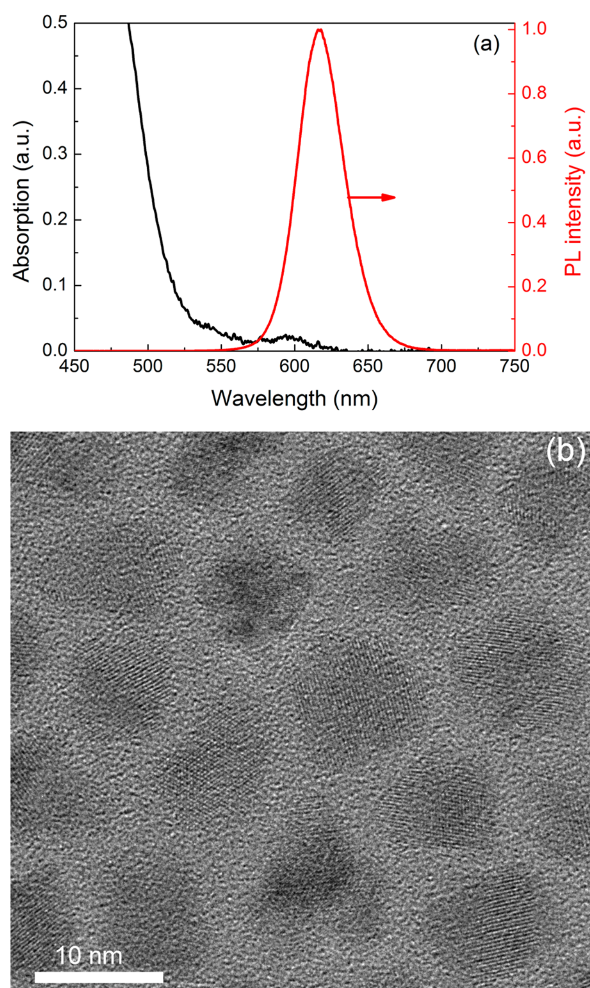

Figure 1. (a) Absorption and PL spectrum of CdSe/ZnS core/shell QDs; (b) TEM image of the CdSe/ZnS core/shell QDs. The scale bar is 10 nm.

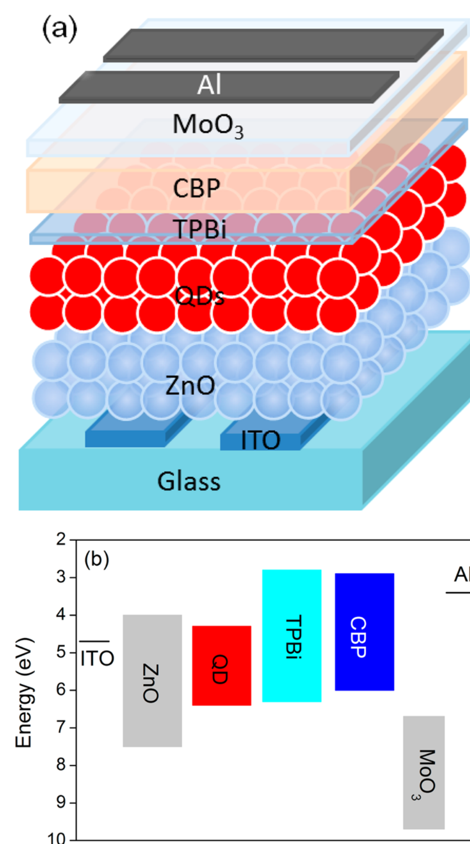

Figure 2. (a) Schematic structure of the QD-LED; (b) flat energy level diagram of the materials used in this study.

order of magnitude of 1×10^{-5} cm^2 V^{-1} s^{-1}. The hole mobility of n-type matrix materials are typically at least 1 order of magnitude lower than their electron mobility.[27] The hole mobility of TPBi should be less than 1×10^{-5} cm^2 V^{-1} s^{-1}, which results in a hole barrier when TBPi is inserted at CBP/QDs interface. Consequently, the charge accumulated interface should be moved to CBP/TPBi interface, which makes the exciton recombination zone away from the charge accumulation interface, suppressing the exciton quenching processes as can be seen from the energy level diagram in Figure 2b.

Images a and b in Figure 3 show the SEM images of the ITO/ZnO and ITO/ZnO/QDs, respectively. As can be seen from Figure 3a, a homogeneous ZnO layer is obtained on ITO substrate. In fact, the ZnO layer is not always perfect. Some streaks of imperfections and voids are observed. However, after spin-coating a QD solution, a high-quality close-packed QD film is obtained as can be seen from Figure 3b. As we know, a high-quality QD film is the prerequisite to build an efficient QD-LED. The thicknesses of ZnO (~45 nm) and QD (~30 nm) layers are obtained through the cross-section SEM images of ITO/ZnO and ITO/ZnO/QDs samples, and data are not shown here.

Figure 4a shows the current density−voltage−luminance characteristics of all the devices with and without the TPBi interlayer. We can see that the current density is decreased at the same operating voltage with increasing the TPBi thickness, which is due to the lower hole mobility of TPBi than that of CBP and the hole injection barrier at the CBP/TPBi interface as seen in Figure 2b. The current density is decreased from 205 mA/cm^2 for Device A (with 0 nm TPBi) to 72 mA/cm^2 for Device E (with 7 nm TPBi) at voltage of 5 V. We can also observe that the introduction of TPBi layer increases the operation voltage at the same luminance level in QD-LEDs However, the maximal luminance is similar, >20 000 cd/m^2 for both the conventional and TPBi-containing devices except for the 7 nm TPBi device.

Figure 4b shows the current density−efficiency properties of all of QD-LEDs. As can be seen, the current efficiency is largely enhanced, especially at low current density region (<100 mA/cm^2), with increasing TPBi thickness until the thickness reaches to 7 nm. The maximal current efficiency is 13.1 cd/A for Device D with a 3.5 nm TPBi interlayer, a 46% enhancement is achieved compared to the conventional Device A, of which the peak current efficiency is 9.0 cd/A. Figure 4c shows the voltage−power efficiency curves of QD-LEDs. The maximal power efficiency is obtained at higher operation voltage with TPBi introduction due to the barrier to hole injection at CBP/TPBi interface and inferior hole transport ability of TPBi. However, the maximum of power efficiency is 9.5 lm/W for the conventional device (Device A), which is increased to 11.7 lm/W for Device D (with 3.5 nm TPBi interlayer). The efficiencies of QD-LEDs at different luminance are also shown in Figure 4d. We can see that the efficiency of Device D is always higher than that of Device A at the luminance range of 10 to 10 000 cd/m^2. We repeated all the above experiments and the results indicated that the introduction of TPBi interlayer into the QD-

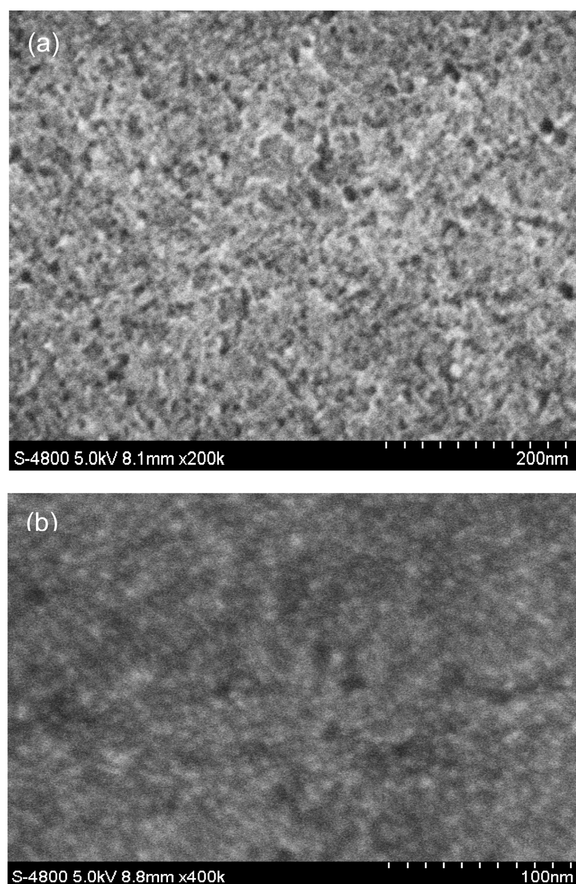

Figure 3. SEM images of (a) ITO/ZnO and (b) ITO/ZnO/QDs.

LEDs substantially enhanced the device performance. It is also important to note that this significant improvement is achieved with a rather simple device structure and without sacrificing the operation voltage and power efficiency. Therefore, the underlying mechanisms that lead to this improvement need to be deeply investigated, as it could provide useful design guidelines for high efficiency QD-LEDs. We can see that there is not any difference between the devices except for the TPBi interlayer in Devices B–D compared to Device A. The TPBi interlayer could have three effects on the devices: the first one is that it decreases the amount of holes injected into QDs, which may improve the electron/hole balance in QDs; the second one is that it separates the charge accumulation interface of TPBi/CBP from the exciton recombination zone TPBi/QDs; and the last one is that it changes the electric field distributions near the QDs because of the different surrounding conditions for QDs in with and without TPBi devices. All of these effects will influence the device performance and need to be investigated in detail.

To assess the effect induced by the charge injection (i.e., the first effect of TPBi considered above), we fabricated a QD-LED with bis(4,6-difluorophenylpyridinato-N,C2)picolinatoiridium (FIrpic) to substitute for TPBi. The experiment results indicated that the device peak efficiency was decreased with the FIrpic introduction as shown in Figure 5. The FIrpic, similar to TPBi, also possesses a lower hole mobility than that of CBP and can decrease the amount of holes injected into QDs. But the higher HOMO level (5.8 eV) of FIrpic than that of CBP results in the charges to accumulate at FIrpic/QD interface, which quenches the excitons on QDs. These results demonstrate that the improvement of device performance does not originate from the change of charge injection into the QD layer. Further, we measured the PL decay of QD layer to explore the influence of electric field on the dynamics process of excitons formed within QDs. As shown in Figure 6 and Table 1, the lifetimes (τ) of excitons on QDs in Device A and Device D are all shortened compared to that of excitons formed on QDs on glass substrate, which may be due to the QD charging effect or/and electron transfer processes when QDs directly contact with ZnO nanoparticle layer. It is worth noting that the lifetimes of QD excitons in Devices A and D is almost the same at bias from 1.7 V to −2 V, which eliminates the effect of varying electric field induced by TPBi on the exciton decay. We also measured the lifetimes of excitons on QDs in Devices B, C, and E at different bias from 1.7 V to −2 V and similar results were obtained that the exciton lifetimes were not correlated with the electric field. In other words, the bias applied on the devices has hardly effect on the exciton decay. Similar phenomenon was also observed by Kilimov group.[3] This is ascribed to the thick ZnS shell, which provides a large barrier to both holes and electrons and suppresses the QD charging processes. As concerned above, we can conclude that the improvement of the device performance should come from the decreased quenching processes caused by radical cations (or accumulated holes) at the QD/organic layer interface, but not from the changes of charge injection or electric field distributions. The introduction of TPBi interlayer suppresses the quenching processes and enhances the device performance by separating the exciton formation zone from the charge accumulated interface.

According to the analysis above, Device A should be a hole-dominant device because of the low electron mobility of QD layer. To deeply understand the influence of TPBi thickness on device performance, we analyze the charge density at the TPBi/QD interface. The neat surface charge density at the QD/organic layer interface can be expressed as in following equation

$$\sigma = \sigma_h - \sigma_e = \varepsilon_{r1}\varepsilon_0 E_A - \varepsilon_{r2}\varepsilon_0 E_C$$

Where σ_e (σ_h) is the surface density of electrons (holes) at the QDs/organic layer interface, ε_{r1} and ε_{r2} are the relative dielectric constants of organic layer and QD layer, respectively. Here, the relative dielectric constants of all of organic materials are supposed to be the same. ε_0 is the vacuum dielectric constants, and E_{CBP} and E_{TPBi} are the electric field in the organic layers of CBP and TPBi layers, respectively. E_A is the total of E_{CBP} and E_{TPBi} and E_C represents the total electric field in QD and ZnO layers. σ_e and E_C are presumably constants for a given current density in all the devices because the ZnO and QD layers are the same for all of the QD-LEDs. Under a given current density, E_{CBP} is presumably constant for a given current density in all the devices because the CBP thickness is constant. The introduction of the TPBi layer into the device will lead to an accumulation of holes at the CBP/TPBi interface and hence increase the electric field in the TPBi layer, which will increase the E_A and then causes σ_h to decrease proportionally. Accordingly, charge quenching caused by σ_h is reduced and the current efficiency is enhanced. Increasing TPBi thickness will result in a higher electric field in TPBi, hence further increasing the E_A, which will lead to neat surface negative charges due to the large decrease in holes at TPBi/QD interface. In addition, a thicker TPBi will result in a unbalanced hole/electron injection into QDs due to the inferior hole

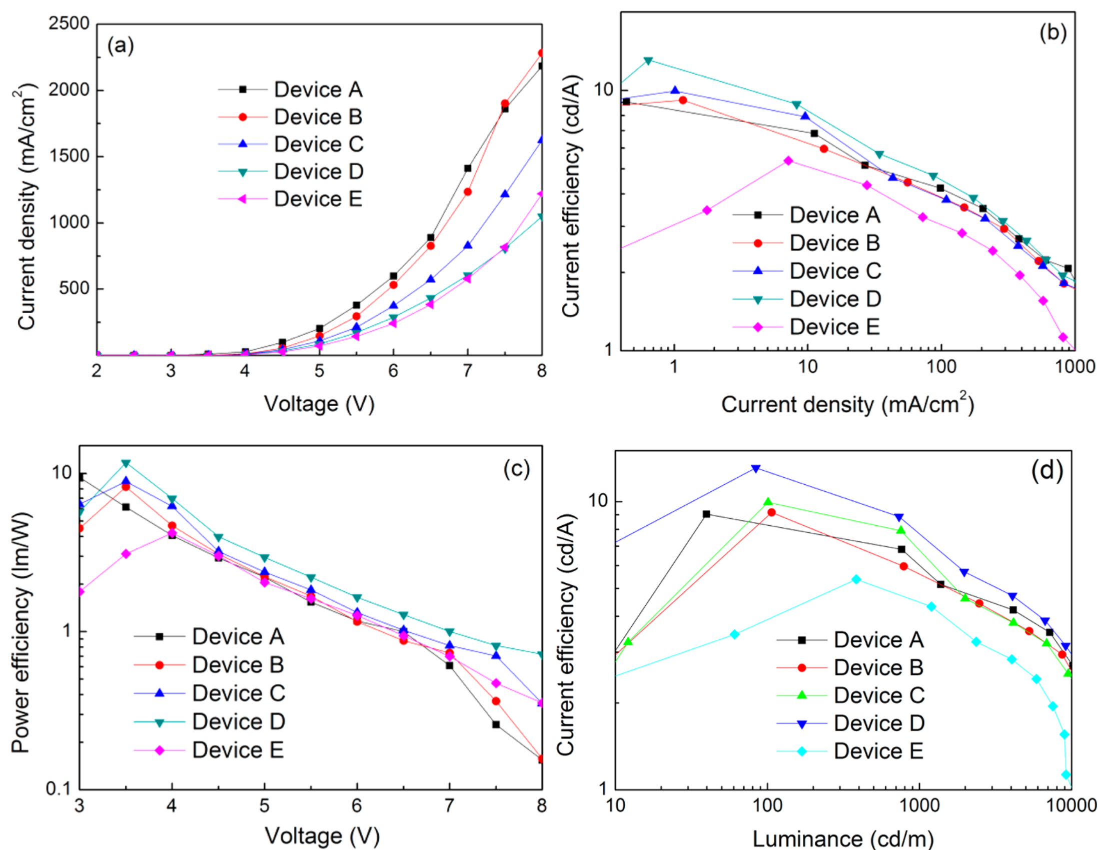

Figure 4. (a) Current density−voltage and (b) efficiency−current density curves of all the devices; (c) voltage−power efficiency and (d) efficiency−luminance properties of all the devices.

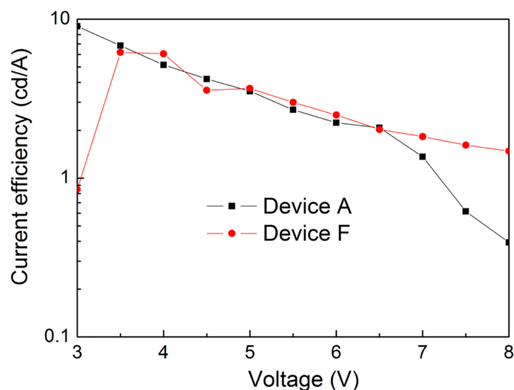

Figure 5. Efficiency-voltage properties of Device A and Device F. Device F consists of ITO/ZnO (45 nm)/QDs (30 nm)/FIrpic (3 nm)/CBP (50 nm)/MoO_3 (5 nm)/Al (100 nm).

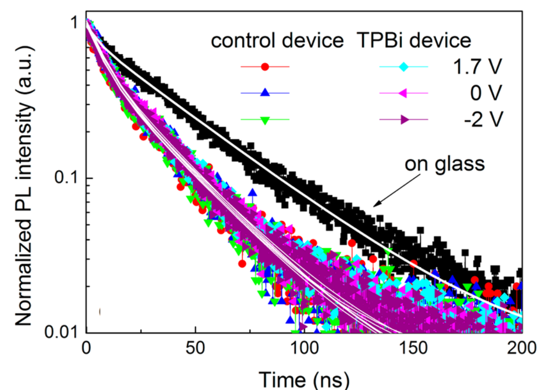

Figure 6. Transient PL dynamics characteristics of the QD layer on glass substrate and in devices at different bias. The white lines represent the fitting curves fitted by a two-exponential model.

mobility of TPBi. These two effects decrease the device performance as seen in Device E with a 7 nm TPBi interlayer.

Figure 7a shows the EL spectra of all the QD-LEDs at a half-exponential coordinates to clearly exhibit EL components in the whole visible region. We can see that there is not any broadening feature or emission at the low-energy region in the EL spectrum for each device, demonstrating the absence of emission from deep-level trap states. In addition, the commonly parasitic EL emission from the adjacent organic layers is also not observed even at higher operation voltage of 6 V as seen in Figure 7b. All of the results indicate that the excitons are dominantly formed on QDs in our QD-LEDs. In addition, it is reported that the interface dipole formed at TPBi/HTL interface would shift down the LUMO level of TPBi.[20] The lower LUMO level of TPBi is of benefit to the hole injection into the QDs, combined with the easier injection pathway for electrons into QDs, which results in efficient formation of the excitons on QDs. The inset of Figure 7a shows the comparison

Table 1. Lifetime of QDs in Different Devices and Bias, As Well As QDs on Glass Substrate

samples	τ at 1.7 V (ns)	τ at 0 V (ns)	τ at −2 V (ns)
Device A	25.5	24.9	25.6
Device D	26.5	26.3	26.6
on glass		40.4	

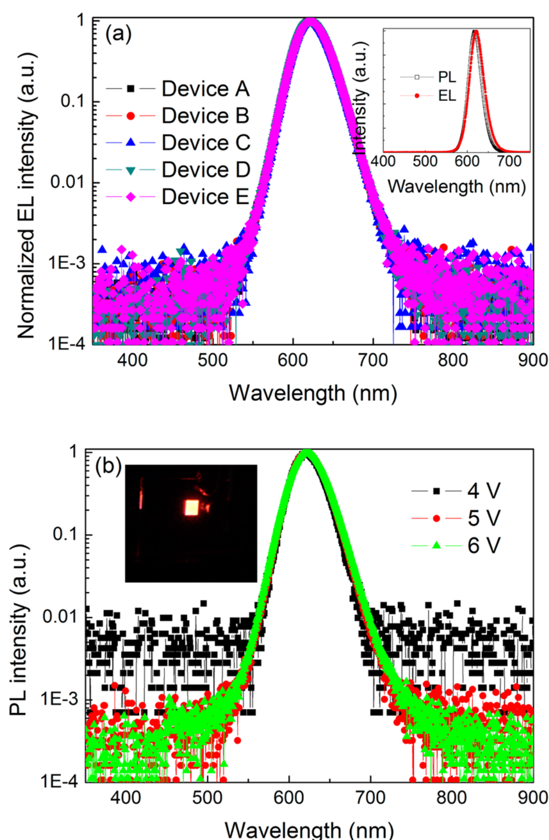

Figure 7. (a) EL spectra of all of the QD-LEDs. The inset shows the EL (for Device D at 5 V) and PL spectra; (b) EL spectra of Device E at different voltages. All the EL spectra are shown at half-exponential coordinates to clearly exhibit EL components.

between PL and EL spectra, whereas the latter is obtained from the QD solution prior to device fabrication. The EL spectrum is almost consistent with the PL one, and the fwhm of EL spectra is 40 nm for all the devices, only a little larger than that of PL, which is about 37 nm. This well complete PL-EL spectral overlap is consistent with the fact that the QD film is the only component of our QD-LEDs for EL. Moreover, there is only a small red-shift for the EL spectrum as compared to the PL spectrum, the emission peaks are 620 and 618 nm for EL and PL spectrum, respectively. In general, the red-shift for the EL spectrum relative to PL spectrum is due to the energy transfer between the QDs in QD film. In our QD materials, the thick ZnS shell outside the CdSe core reduces the energy transfer process between QDs and, to a large extent, decreases the red-shift. The EL spectra shown in Figure 7b are obtained at different bias from 4 to 6 V for Device D, and the inset is the photograph of Device D at an operating voltage of 4 V. We can see that the properties, including emission peak, fwhm, and distribution, are independent of the bias applied to the device, which further indicates that the luminescence properties are not affected by the electric field because of the very thick ZnS shell coated outside the CdSe core in the CdSe/ZnS QDs used in our study. These results are in good agreement with the above analysis about the exciton lifetime as shown in Figure 5. It is noteworthy that the similar properties between the PL and EL and the stability of QD emission are thanks to the very thick ZnS shell overcoated outside the CdSe core, which also suggests that QDs with a thick wide bandgap shell material should be more suitable to fabricate highly efficient QD-LEDs.

CONCLUSIONS

In summary, we have successfully fabricated highly efficient QD-LEDs with an inverted structure by inserting a TPBi layer at QDs/CBP interface. No emission from organic materials or surface defect/trap states is observed even when a 7 nm TPBi is adopted, which indicates that the excitons are all formed on QDs in our QD-LEDs. An enhancement of 46% for device peak efficiency is achieved with a 3.5 nm TPBi interlayer. This work demonstrates that the position of the QD emission layer (i.e., the exciton formation zone) in QD-LEDs is a crucial factor and the quenching processes caused by accumulated charges at the QDs/CBP interface dramatically decrease the device efficiency. Clearly the traditional concept of confining holes and electrons at the emission interface is not an optimal device design option as reported in OLEDs by Lu group.[20] We have demonstrated that exciton quenching due to accumulated space charges at the exciton formation interface remains a significant loss of efficiency in common devices. The device performance will be further enhanced by carefully controlling the exciton formation zone and improving the charge balance injected into the QD emission layer.

AUTHOR INFORMATION

Corresponding Authors

*E-mail: jpt86@163.com.

* E-mail: zhaojl@ciomp.ac.cn.

Notes

The authors declare no competing financial interest.

ACKNOWLEDGMENTS

This work was supported by National Natural Science Foundation of China (61205025, 11274304, 51103144, 61274126, 61275197, and 11204298) and Project supported by State Key Laboratory of Luminescence and Applications, SKKLLA201303.

REFERENCES

(1) Mashford, B. S.; Stevenson, M.; Popovic, Z.; Hamilton, C.; Zhou, Z.; Breen, C.; Steckel, J.; Bulović, V.; Bawendi, M.; Coe-Sullivan, S.; Kazlas, P. T. High-efficiency Quantum-dot Light-emitting Devices with Enhanced Charge Injection. *Nat. Photonics* **2013**, *7*, 407−412.

(2) Kwak, J. H.; Bae, W. K.; Lee, D. G.; Park, I.; Lim, J. H.; Park, M. J.; Cho, H. D.; Woo, H. J.; Yoon, D. Y.; Char, K. H.; Lee, S. H.; Lee, C. H. Bright and Efficient Full-Color Colloidal Quantum Dot Light-Emitting Diodes Using an Inverted Device Structure. *Nano Lett.* **2012**, *12*, 2362−2366.

(3) Bae, W. K.; Park, Y.-S.; Lim, J.; Lee, D.; Padilha, L. A.; McDaniel, H.; Robel, I.; Lee, C.; Pietryga, J. M.; Klimov, V. I. Controlling the Influence of Auger Recombination on the Performance of Quantum-dot Light-emitting Diodes. *Nat. Commun.* **2013**, *4*, 2661.

(4) Colvin, V. L.; Schlamp, M. C.; Alivisatos, A. P. Light-Emitting-Diodes Made from Cadmium Selenide Nanocrystals and a Semi-conducting Polymer. *Nature* **1994**, *370*, 354−357.

(5) Coe, S.; Woo, W.-K.; Bawendi, M. G.; Bulović, V. Electro-luminescence from Single Monolayers of Nanocrystals in Molecular Organic Devices. *Nature* **2002**, *420*, 800−803.

(6) Sun, Q.; Wang, Y. A.; Li, L. S.; Wang, D.; Zhu, T.; Xu, J.; Yang, C.; Li, Y. Bright, Multicoloured Light-emitting Diodes Based on Quantum Dots. *Nat. Photonics* **2007**, *1*, 717−722.

(7) Tan, Z.; Zhang, F.; Zhu, T.; Xu, J.; Wang, A. Y.; Dixon, J. D.; Li, L.; Zhang, Q.; Mohney, S. E.; Ruzyllo, J. Bright and Color-saturated Emission from Blue Light-emitting Diodes bBased on Solution-processed Colloidal Nanocrystal Quantum Dots. *Nano Lett.* **2007**, *7*, 3803−3807.

(8) Anikeeva, P. O.; Halpert, J. E.; Bawendi, M. G.; Bulović, V. Quantum Dot Light-Emitting Devices with Electroluminescence Tunable over the Entire Visible Spectrum. *Nano Lett.* **2009**, *9*, 2532−2536.

(9) Cho, K.-S.; Lee, E. K.; Joo, W.-J.; Jang, E.; Kim, T.-H.; Lee, S. J.; Kwon, S.-J.; Han, J. Y.; Kim, B.-K.; Choi, B. L.; Kim, J. M. High-performance Crosslinked Colloidal Quantum-dot Light-emitting Diodes. *Nat. Photonics* **2009**, *3*, 341−345.

(10) Shen, H.; Bai, X.; Wang, A.; Wang, H.; Qian, L.; Yang, Y.; Titov, A.; Hyvonen, J.; Zheng, Y.; Li, L. S. High-Efficient Deep-Blue Light-Emitting Diodes by Using High Quality $Zn_xCd_{1-x}S$/ZnS Core/Shell Quantum Dots. *Adv. Funct. Mater.* **2014**, *24*, 2367−2373.

(11) Shirasaki, Y.; Supran, G. J.; Bawendi, M. G.; Bulović, V. Emergence of Colloidal Quantum-dot Light-emitting Technologies. *Nat. Photonics* **2013**, *7*, 13−23.

(12) Matioli, E.; Brinkley, S.; Kelchner, K.; Hu, Y.; Nakamura, S.; DenBaars, S.; Speck, J.; Weisbuch, C. High-brightness Polarized Light-emitting Diodes. *Light Sci. Appl.* **2012**, *1*, e22.

(13) Xiang, C.; Koo, W.; So, F.; Sasabe, H.; Kido, J. A Systematic Study on Efficiency Enhancements in Phosphorescent Green, Red and Blue Microcavity Organic Light Emitting Devices. *Light Sci. Appl.* **2013**, *2*, e74.

(14) Anikeeva, P. O.; Madigan, C. F.; Halpert, J. E.; Bawendi, M. G.; Bulović, V. Electronic and Excitonic Processes in Light-emitting Devices Based on Organic Materials and Colloidal Quantum Dots. *Phys. Rev. B* **2008**, *78*, 085434.

(15) Mueller, A. H.; Petruska, M. A.; Achermann, M.; Werder, D. J.; Akhadov, E. A.; Koleske, D. D.; Hoffbauer, M. A.; Klimov, V. I. Multicolor Light-emitting Diodes Based on Semiconductor Nano-crystals Encapsulated in GaN Charge Injection Layers. *Nano Lett.* **2005**, *5*, 1039−1044.

(16) Kim, T.-H.; Cho, K.-S.; Lee, E. K.; Lee, S. J.; Chae, J.; Kim, J. W.; Kim, D. H.; Kwon, J.-Y.; Amaratunga, G.; Lee, S. Y.; Choi, B. L.; Kuk, Y.; Kim, J. M.; Kim, K. Full-colour Quantum Dot Displays Fabricated by Transfer Printing. *Nat. Photonics* **2011**, *5*, 176−182.

(17) Qian, L.; Zheng, Y.; Xue, J.; Holloway, P. H. Stable and Efficient Quantum-dot Light-emitting Diodes Based on Solution-processed Multilayer Structures. *Nat. Photonics* **2011**, *5*, 543−548.

(18) Cheng, K.-Y.; Anthony, R. U.; Kortshagen, R.; Holmes, R. J. High-Efficiency Silicon Nanocrystal Light-Emitting Devices. *Nano Lett.* **2011**, *11*, 1952−1956.

(19) Ji, W.; Jing, P.; Zhao, J. Improving the Efficiency and Reducing Efficiency Roll-off in Quantum Dot Light Emitting Devices by Utilizing Plasmonic Au Nanoparticles. *J. Mater. Chem. C* **2013**, *1*, 470−476.

(20) Wang, Z. B.; Helander, M. G.; Liu, Z. W.; Greiner, M. T.; Qiu, J.; Lu, Z. H. Controlling Carrier Accumulation and Exciton Formation in Organic Light Emitting Diodes. *Appl. Phys. Lett.* **2010**, *96*, 043303.

(21) Ji, W. Y.; Jing, P. T.; Zhao, J. L.; Liu, X.; Wang, A.; Li, H. Inverted CdSe/CdS/ZnS Quantum Dot Light Emitting Devices with Titanium Dioxide as an Electron-injection Contact. *Nanoscale* **2013**, *5*, 3474−3480.

(22) Ji, W. Y.; Zhang, L. T.; Gao, R. X.; Zhang, L. M.; Xie, W. F.; Zhang, H. Z.; Li, B. Top-emitting white organic light-emitting devices with down-conversion phosphors: Theory and experiment. *Opt. Express* **2008**, *16*, 15489−15494.

(23) Shen, H.; Lin, Q.; Wang, H.; Qian, L.; Yang, Y.; Titov, A.; Hyvonen, J.; Zheng, Y.; Li, L. S. Efficient and Bright Colloidal Quantum Dot Light-Emitting Diodes via Controlling the Shell Thickness of Quantum Dots. *ACS Appl. Mater. Interfaces* **2013**, *5*, 12011−12016.

(24) Ji, W. Y.; Jing, P.; Xu, W.; Yuan, X.; Wang, Y.; Zhao, J.; Jen, A. K.-Y. High Color Purity ZnSe/ZnS Core/shell Quantum Dot Based Blue Light Emitting Diodes with an Inverted Device Structure. *Appl. Phys. Lett.* **2013**, *103*, 053106.

(25) Pal, B. N.; Ghosh, Y.; Brovelli, S.; Laocharoensuk, R.; Klimov, V. I.; Hollingsworth, J. A.; Htoon, H. 'Giant' CdSe/CdS Core/Shell Nanocrystal Quantum Dots As Efficient Electroluminescent Materials: Strong Influence of Shell Thickness on Light-Emitting Diode Performance. *Nano Lett.* **2012**, *12*, 331−336.

(26) Xu, W.; Ji, W. Y.; Jing, P.; Yuan, X.; Wang, Y. A.; Xiang, W.; Zhao, J. Efficient Inverted Quantum-dot Light-emitting Devices with TiO_2/ZnO Bilayer as the Electron Contact Layer. *Opt. Lett.* **2014**, *39*, 426−429.

(27) Baek, H.; Lee, C. H. Electroluminescence Characteristics of n-type Matrix Materials Doped with Iridium-based Green and Red Phosphorescent Emitters. *J. Appl. Phys.* **2008**, *103*, 054510.